Lasers in Manufacturing Conference 2019

Distinct changes in microstructure due to heat input during laser metal deposition of H13 tool steel

Bohlen, A.[a*], Freiße, H.[a], Vollertsen, F.[a,b]

[a]*BIAS - Bremer Institut für angewandte Strahltechnik, Klagenfurter Str. 5, 28359 Bremen, Germany*
[b]*University of Bremen, Bibliothekstr. 1, 28359 Bremen, Germany*

Abstract

Additive manufacturing offers many benefits, especially for expensive tools. Laser metal deposition is an economically profitable manufacturing process for the generation of tools, due to high achievable build rates and unrestricted build volume. In a layer by layer deposition the already deposited layers will be reheated and cooled numerous times and therefore will have multiple phase transformations. Heat accumulation during the process will lead to changing cooling rates, which have a direct impact on microstructure. Building strategies have an influence on the thermal history due to the changes in heat accumulation within the part. Thus, different building strategies lead to different distribution in the microstructure. In this study thin walled specimen made by laser metal deposition from H13 tool steel were investigated. Different building strategies were used, as well as different pause times between single layers. Sharp transitions in microstructure were detected, which softened with higher energy input per time.

Keywords: Additive Manufacturing; Laser Metal Deposition; H13 Tool Steel; FEM Simulation

1. Introduction

Additive manufacturing techniques for the production of metal components have a growing importance for industrial applications. Melting material with a laser results in a low dilution of the underlying material and low residual stresses. Laser metal deposition (LMD) is an open space process in which the material is deposited layer by layer. The applications areas are the repair of existing tool surfaces (Nowotny et al., 2007), surface coating for higher wear resistance (Köhler et al., 2014) or the 3D generation of new

* Corresponding author. Tel.: +49-421-218-58110; fax: +49-421-218-58063.
E-mail address: bohlen@bias.de

components (Freiße et al., 2015). LMD can produce high density parts, making this process suitable to produce tools or dies. Challenges during manufacturing, which still need to be addressed, include the local variation of the heat transfer rates during the process (Schmidt et al., 2017). These changing thermal conditions lead to changes in microstructure (Farshidianfar et al., 2016) and therefore in hardness distribution. High cooling rates can occur during the LMD process, on cold substrates they can be up to 10^4 K/s (Zheng et al., 2008). High temperature gradients induce residual stresses (Neugebauer et al., 2014) and thus can have a negative impact on the quality of parts, for example on the shape accuracy in thin-walled parts (Papadakis, Hauser, 2017).

The hot work tool steel H13 (DIN EN X40CrMoV5-1 or 1.2344) is commonly used for hot-forging tools, die-casting dies or hot extrusion tools, because of its toughness and high hot hardness (Roberts et al., 1998). In LMD coatings of H13 the microstructure consists of martensite, retained austenite and fine carbides leading to a hardness of up to 650 HV (Telasang et al., 2014). In single pass walls made of H13 via LMD the lower layers indicate a more tempered structure, caused by more re-heating (Hofmeister, Griffith, 2001). In solid parts the top layer showed a fine martensitic microstructure and a high hardness of 580 HV to 650 HV. Lower layers showed a tempered microstructure and hardness values as low as 278 HV (Cottam et al., 2014). Brooks et al., 1999 divided single line width parts into three different thermal regions. The region located from the top of the specimen is supposedly heated above 925 °C in the last cycle leading to an untempered martensitic microstructure without carbides. The second region is a transition zone with approximately single pass height followed by a region of tempered martensite with fine V-carbides and larger Cr-carbides. Pinkerton, Li, 2005 also divided single line width parts into three different regions. The top surface shows high hardness, further from the top at the transition region a decrease in hardness is found. At further distance from the top an increase in hardness is detected, assumingly due to secondary hardening.

Different regions of microstructure have been reported for H13 tool steel, as well as the correlating changes in hardness associated with the microstructure. However, pauses during build-up have not been considered for LMD and thus their influence on the depth of tempering in the build part. In this study different pauses between reheating will be investigated for thin-walled specimens and if a FEM simulation with commercial welding software can predict the hardness penetration depth.

2. Experimental

2.1. Material

The hot work tool steel H13 (DIN EN X40CrMoV5-1 or 1.2344) was used in the form of spherical powder with a particle diameter between 50 µm and 100 µm, according to manufacturer specifications. The chemical composition of the powder batch is shown in Table 1. To avoid blockage within the powder nozzle the powder was sieved using 45 µm and 100 µm mesh sized sieves. The substrate material on which the powder was deposited is H13 as well to prevent dilution with other materials. The melting temperature of H13 is at 1420 °C. The temperatures of Ac_{1b} and Ac_{1e} are 860 °C and 940 °C, respectively (*StahlWissen - NaviMat*, 2017). Beginning of martensite M_s is at approximately 350 °C (Bohlen et al., 2018). The hardness of annealed H13 is 240 HV, through conventional hardening it can reach hardness values of up to 620 HV. Thermal conductivity after hardening and tempering is 25.5 W/(m·K) at 20 °C and rises to 30.3 W/(m·K) at 700 °C (Abrams Premium Stahl).

Table 1: Chemical composition of used H13 powder analyzed by laser diffraction.

Element	C	Si	Mn	V	Cr	Mo	Fe
Weight percentage	0.4	1.1	0.47	1.0	5.3	1.4	bal.

2.2. Procedure

For laser metal deposition of thin-walled specimens a 4 kW Trumpf HL 4006 Nd:YAG laser with a fiber diameter of 600 µm was used. Collimation length was 150 mm and 200 mm as focusing length. The laser spot in the working plane has a calculated size of 1.5 mm and laser spot is above working plane to avoid dilution. Powder is supplied to the process via a continuous coaxial powder nozzle from Fraunhofer ILT with a constant powder feed rate of 4 g/min. Argon was used as shielding gas with 7.5 l/min and as carrier gas with 2.5 l/min. All thin-walled specimens were deposited using 400 W laser beam power and 800 mm/min welding speed. Length of the build specimens was 40 mm. Vertical spacing was kept constant at 350 µm. The substrate is 50 mm × 17 mm × 10 mm in dimension. The two short faces were sawn, the others milled to ensure consistent positioning. For each parameter variation three specimens were manufactured. Table 2 gives an overview over the different process variants, which were examined. The parts are single line width parts with unidirectional or bidirectional build strategies. The pause between layers was varied as well. Pause times between layers include the set pause in the CNC controller plus pause time from positioning. Type K thermocouples with a wire diameter of 0.13 mm from Omega were used for temperature measurement during the process. The thermocouples were spot welded to the substrate at a distance of 1 mm to the middle of the part, on either side, previous to the process. Temperature was recorded using National Instrument module NI-9212 and LabVIEW software.

Table 2: Overview of studied variation of build direction, pause between layers and number of layers and the resulting build time

variant	build strategy	build time per layer in s	pause between layers in s	layers	build time in s
s	bidirectional	3	0.9	30	116
m	unidirectional	3	2.7	30	168
l	unidirectional	3	12.7	30	458

Samples were taken from the middle of each specimen (Fig. 2) and were then embedded, grinded and polished. After hardness measurement they were etched using Kalling II etchant for 10 s. Microstructure is examined using a Zeiss type AX10 microscope. Height, width and position of change in microstructure was measured using Stream Enterprise software. Vickers hardness was measured using a DuraScan 50 G5 hardness tester from Struers. All measurements were conducted using HV0.5. Indentations were made with 0.5 mm distance starting from the substrate surface and afterwards checked to ensure that no pores or other defects were measured.

2.3. FEM Simulation

The FEM simulations were carried out using the commercial software Simufact.welding (7.2) to calculate a thermal solution. For the simulation CAD geometries were meshed using the Simufact internal meshing

module. The substrate was 50 mm in length, 8.5 mm in width and 10 mm in height, which is half the size of the substrate used in experiments since a symmetry plane was used in the simulation for faster calculation. For the deposited layers the CAD geometry had a height of 0.35 mm, which is equal to the z-increment per layer. The length is 40 mm and width 0.5 mm. The width was derived from single track cross sections. Each layer geometry consists of 640 elements. The whole model consists of approximately 20500 elements. The heat source is based on beam measurements and cross sections of single track. The heat source diameter is 1.5 mm, power is set to 400 W with an efficiency factor of 0.6. The position of the heat source was on top of the currently build layer. Particles were set on top of each layer in the middle of the length of the track, to get a temperature output for these points.

The simulation was compared to the thermocouple measurements to ensure the comparability of the simulations to the experiments (Fig. 1). The temperature peaks were not primarily used to compare the simulation with the experiments, nut instead the cooled down temperatures in each layer. Peak temperatures for the experiments are dependent on the response time of the thermocouples and for simulations the mesh of the geometry affects the reached peak temperature. They were in good agreement with the measured temperatures. For each layer height and temperature cycle it was evaluated if Ac_{1e} temperature was reached during heat up and if M_s temperature was reached while cooling down.

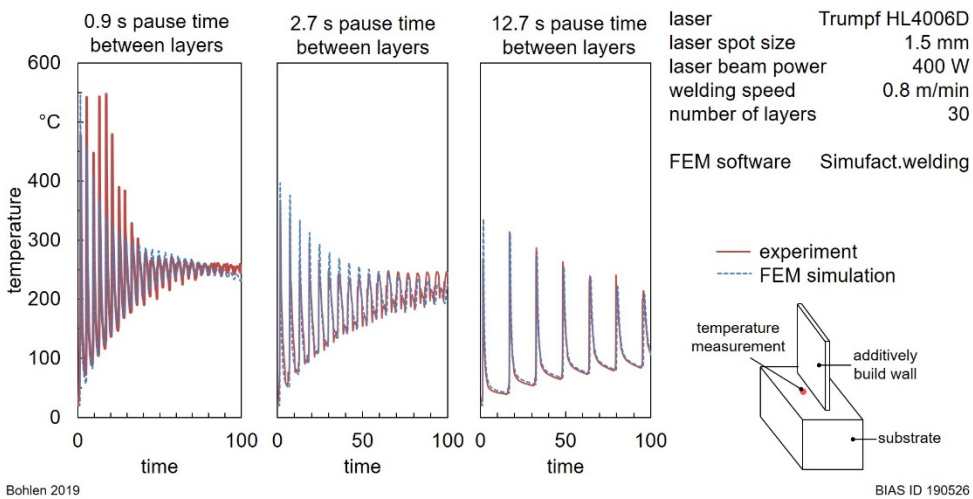

Fig. 1: Comparison between measured temperature at the substrate and calculated temperature with Simufact.welding.

3. Results

3.1. Laser Metal Deposition

In Fig. 2 etched cross sections for each variant are depicted. The strongest visual distinctive change in microstructure can be seen for the specimens with 12.7 s of pause time between layers. The total height for this variant is 10.8 mm ± 0.1 mm and the change in microstructure is at 9.0 mm ± 0.1 mm. The height of specimens with a pause time of 2.7 s is 10.5 mm ± 0.1 mm and for 0.9 s pause time 10.7 mm ± 0.1 mm. The

optical changes in microstructure in these two variants are not as distinct. For 2.7 s pause time it is at an approximated height of 2.5 mm and for 0.9 s pause time at 1.3 mm.

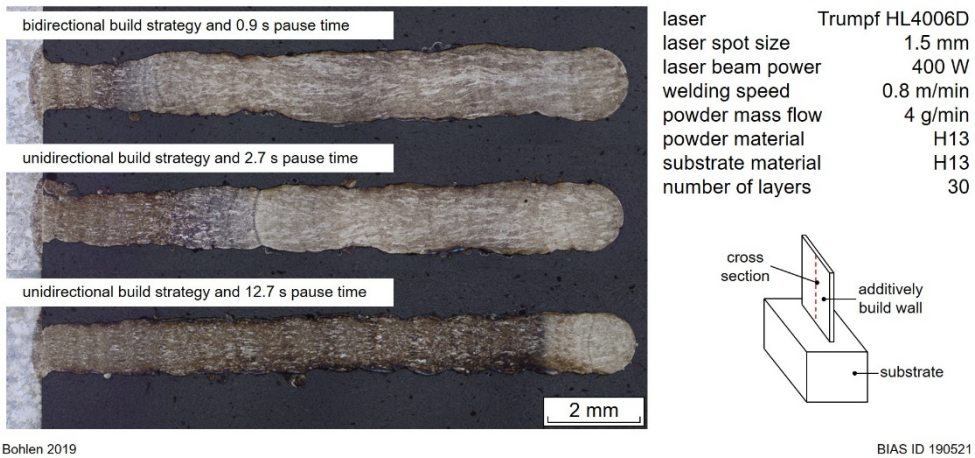

Fig. 2: Cross sections etched with Kalling II reagent, from top to bottom are variants s, m and l, and a specimen with indicated cutting plane.

The hardness values, which can be seen in Fig. 3, are portrayed over the distance to the substrate. Hardness in the substrate is approximately 200 HV0.5 for each variant. In the first 1.5 mm of the build structure each variant shows a decrease in hardness values. Values are then increasing again for all variants. For parts with 0.9 s of pause time an increase in hardness starts after 1.5 mm. Maximum measured hardness of 705 HV0.5 ± 36 HV0.5 is at 9 mm.

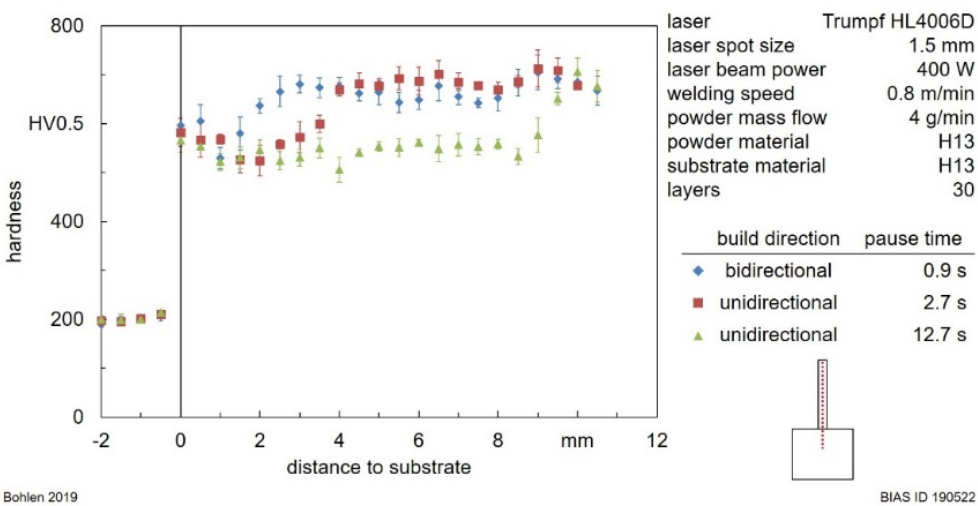

Fig. 3: Hardness distribution for bidirectional and unidirectional build parts with different pause times between layers.

The increase in hardness for specimens with 2.7 s of pause time starts at 2 mm and has its measured maximum at 9 mm with 712 HV0.5 ± 38

3.2. FEM-Simulation

During the deposition the material will reach its melting point and will cool down after deposition. During the cooling phase it will first go beneath the Ac_{1e} (940 °C) temperature and then below M_s (350 °C) temperature. When no layer further layers are deposited the temperature will eventually reach room temperature again. But during the buildup of a 3D part additional layers will interrupt the cooling down of initial layers. It is dependent on the time between deposition and reheating, due to additional layers, if M_s will be reached during cool down. When new layers are added to the part previous layers can reach Ac_{1e} temperature again. With each new layer the previous deposited material will undergo a new thermal cycle, which will have impact on the resulting microstructure.

Fig. 4 shows for simulated parts with 12.7 s pauses between layers if Ac_{1e} and/or M_s was reached in each temperature cycle. When each layer is deposited it will reach Ac_{1e} and surpass M_s when cooling down (indicated in dark red). The first layer (height 0.35 mm) will not reach Ac_{1e} again ongoing from temperature cycle 5 (indicated in orange). In the last temperature cycle Ac_{1e} was still reached 6 layers from the top of the part, until a height of 8.4 mm.

In Fig. 5 it can be seen that for parts with pause times between layers of 2.7 s the first layer will reach Ac_{1e} and M_s for 5 temperature cycles and for the following cycles will only reach M_s. Between temperature cycles 22 and 29 starting at a height of 4.9 mm the specimen will not reach M_s anymore until the cool down after deposition. Some of these layers will reach Ac_{1e} (indicated in bright red), while others do not reach Ac_{1e} anymore (indicated in yellow). After the last temperature cycle every layer will reach M_s again while cooling down to room temperature.

For a pause time of 0.9 s between layers Fig. 6 shows that again the first layers will reach Ac_{1e} for 5 deposition cycles. Starting in cycle 17 the layers from height 1.75 mm upwards will not reach M_s temperature anymore until the final cool down of the part. In cycle 29 between 2.45 mm and 7 mm neither Ac_{1e} or M_s will be reached, from 7.35 mm to the top Ac_{1e} will be surpassed but layers will not cool down to M_s.

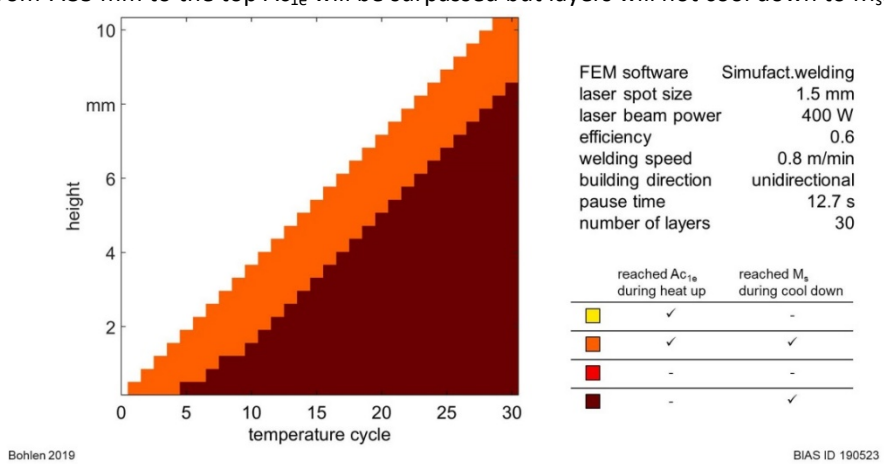

Fig. 4: Reached temperatures for Ac_{1e} and M_s for each layer at each temperature cycle for parts with 12.7 s pause time between layers.

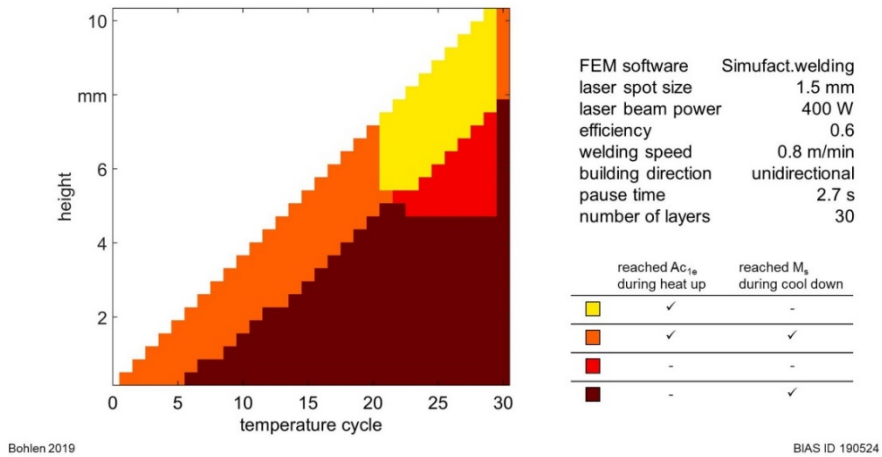

Fig. 5: Reached temperatures for Ac_{1e} and M_s for each layer at each temperature cycle for parts with 2.7 s pause time between layers.

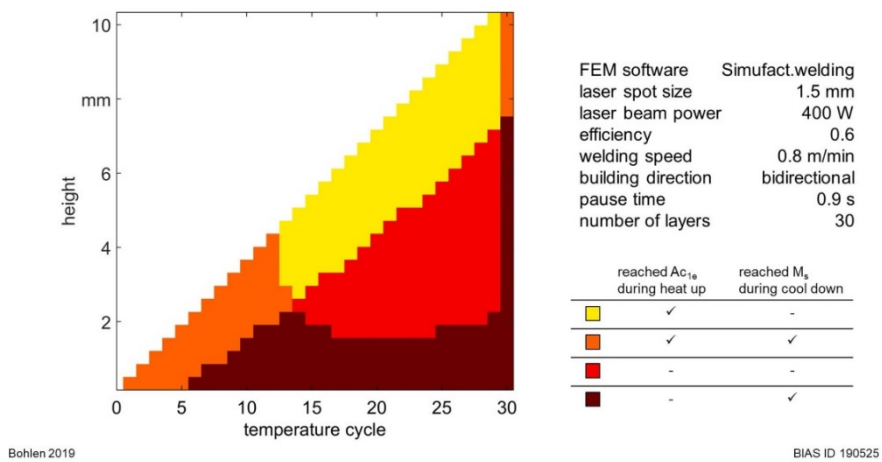

Fig. 6: Reached temperatures for Ac_{1e} and M_s for each layer at each temperature cycle for parts with 0.9 s pause time between layers.

4. Discussion

The three investigated variations of pause time between layers lead to different energy inputs over time. For lower pause times simulations show a pronounced heat accumulation, which is sustained by the thermocouple measurements and the resulting microstructure in the specimens. The simulation of the temperatures for the variation with 12.7 s pause time shows that during the last deposition cycle starting from the height of 8.75 mm these layers will reach Ac_{1e} and thus be austenitized and then rapidly cool down under M_s, building martensite. This is in good agreement with the found microstructure and hardness values which show distinctive changes at 9 mm height. The top 5 to 6 layers in each temperature cycle will reach

Ac_{1e} and because of the long pause time for cooling will reach M_s as well. The layers beneath these will not be austenitized. This could lead to annealed martensite, resulting in a lower hardness.

When the pause times between layers get smaller and thus the energy input per time higher, the thermal history becomes more complex with regard to phase transformations. As opposed to parts with long pauses Fig. 5and Fig. 6 show that due to the heat accumulation some layers will not reach M_s during cool down anymore and thus will not build new martensite until the deposition is finished. In the microstructure for specimens with 0.9 s and 2.7 s of pause times the change in microstructure has a wider transition zone. This is also noticeable in the hardness distribution where the change in hardness is not as distinct as for 12.7 s pause time. The transition in microstructure starts at approximately 1.3 mm for 0.9 s pause time and at 2.5 mm for 2.7 s pause time. For 0.9 s pause time this area correlates with the height 1.75 mm in the simulation where martensite was built during the deposition cycle, but subsequent cycles could neither reach austenitization nor beginning of martensite. For 2.7 s pause times these areas exist as well in the simulation, but their height does not correlate as well with the experiments. In the layers which follow above the beginning of martensite will first be reached after the deposition is finished, due to the heat accumulation. This is in good agreement with the experiments where the upper layers of the specimens show a high hardness leading to the assumption that they have a martensitic microstructure. Further distinctions in the divisions could be made, including the temperature from where the material was heated up during a cycle. It is assumed that this could give more insight into tempering effects.

Overall the thermal FEM simulations are for the most part in good agreement with the found microstructure and hardness values (comparison depicted in Fig. 7).

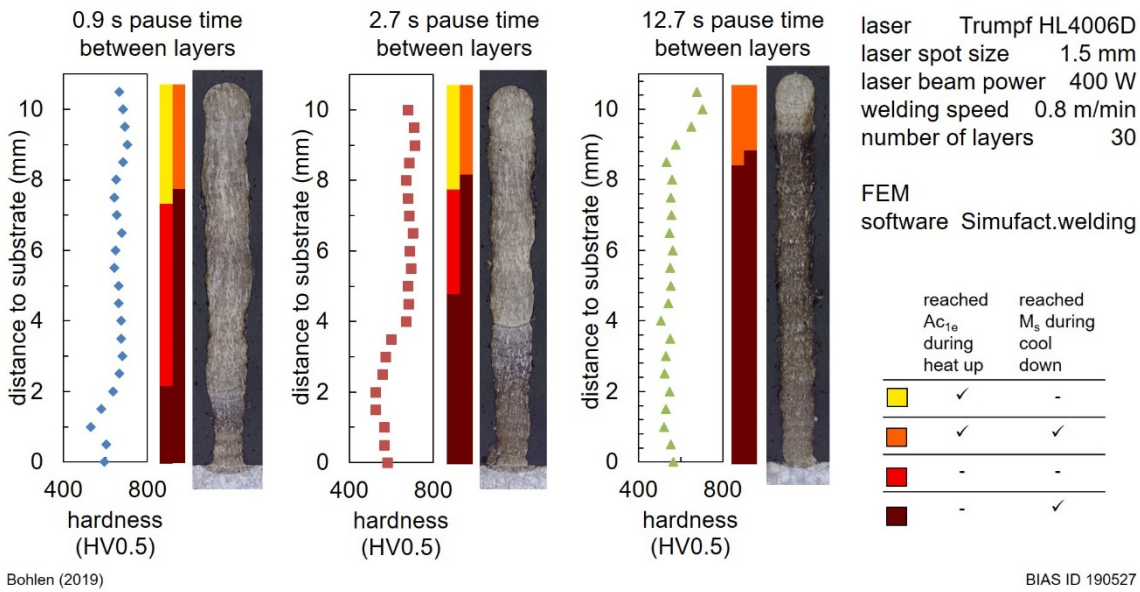

Fig. 7: Comparison of measured hardness values and etched cross sections with the simulated reached temperatures for the last two temperature cycles.

5. Conclusion

Different pause times between single layers were used to investigate distinct changes in microstructure. For lower pause times between layers and thus higher energy input over time the hardness penetration depth increases from 1.7 mm for 12.7 s pause time to 9.3 mm for 0.9 s pause time. Commercial FEM simulations can help determine adapted pause times between layers for a certain hardness penetration depth.

Acknowledgements

The IGF-Project-No.: 19.308 N of the FOSTA - Research Association for Steel Application was funded by the Federal Ministry for Economic Affairs and Energy (BMWi) via the German Federation of Industrial Research Associations (AiF) in accordance with the policy to support the Industrial Collective Research (IGF) on the basis of a decision by the German Bundestag. Furthermore, the authors gratefully acknowledge the collaboration with the members of the project affiliated committee regarding the support of knowledge, material and equipment over the course of the research.

References

Abrams Premium Stahl. Datenblatt 1.2344.

Bohlen, A.; Freiße, H.; Hunkel, M.; Vollertsen, F. Additive manufacturing of tool steel by laser metal deposition. Procedia CIRP 2018, 74, p. 192–195.

Brooks, J.; Robino, C.; Headley, T.; Goods, S.; Griffith, M. Microstructure and Property Optimization of LENS Deposited H13 Tool Steel. Solid Freeform Fabrication Symposium 1999, p. 375–382.

Cottam, R.; Wang, J.; Luzin, V. Characterization of microstructure and residual stress in a 3D H13 tool steel component produced by additive manufacturing. J. Mater. Res. 2014, 29 (17), p. 1978–1986.

Farshidianfar, M. H.; Khajepour, A.; Gerlich, A. P. Effect of real-time cooling rate on microstructure in Laser Additive Manufacturing. Journal of Materials Processing Technology 2016, 231, p. 468–478.

Freiße, H.; Vorholt, J.; Seefeld, T.; Vollertsen, F. Additve Manufacturing of a deep drawing tool by direct laser deposition. Dry Met. Forming OAJ FMT [Online] 2015, No. 1, p. 5–10.

Hofmeister, W.; Griffith, M. Solidification in direct metal deposition by LENS processing. JOM 2001, 53 (9), p. 30–34

Köhler, H.; Rajput, R.; Khazan, P.; Kornmeier, J. R. On the Influence of Laser Cladding and Post-processing Strategies on Residual Stresses in Steel Specimens. Physics Procedia 2014, 56, p. 250–261.

Neugebauer, F.; Keller, N.; Ploshikin, V.; Feuerhahn, F.; Köhler, H. Multi Scale FEM Simulation for Distortion Calculation in Additive Manufacturing of Hardnening Stainless Steel. In Proceedings of the IWOTE'14: International Workshop on Thermal Forming and Welding Distortion; Vollertsen, F., Tetzel, H., Eds.; Strahltechnik 54; BIAS Verlag: Bremen, 2014; p. 13–23.

Nowotny, S.; Scharek, S.; Beyer, E.; Richter, K.-H. Laser Beam Build-Up Welding: Precision in Repair, Surface Cladding, and Direct 3D Metal Deposition. J Therm Spray Tech 2007, 16 (3), p. 344–348.

Papadakis, L.; Hauser, C. Experimental and computational appraisal of the shape accuracy of a thin-walled virole aero-engine casing manufactured by means of laser metal deposition. Prod. Eng. Res. Devel. 2017, 11 (4-5), p. 389–399.

Pinkerton, A. J.; Li, L. Direct additive laser manufacturing using gas- and water-atomised H13 tool steel powders. Int J Adv Manuf Technol 2005, 25 (5-6), p. 471–479.

Roberts, G. A.; Krauss, G.; Kennedy, R. Tool steels, 5th ed.; ASM International: Materials Park, OH, 1998.

Schmidt, M.; Merklein, M.; Bourell, D.; Dimitrov, D.; Hausotte, T.; Wegener, K.; Overmeyer, L.; Vollertsen, F.; Levy, G. N. Laser based additive manufacturing in industry and academia. CIRP Annals 2017, 66 (2), p. 561–583.

StahlWissen - NaviMat; Dr. Sommer Werkstofftechnik GmbH, 2017.

Telasang, G.; Dutta Majumdar, J.; Padmanabham, G.; Tak, M.; Manna, I. Effect of laser parameters on microstructure and hardness of laser clad and tempered AISI H13 tool steel. Surface and Coatings Technology 2014, 258, p. 1108–1118.

Zheng, B.; Zhou, Y.; Smugeresky, J. E.; Schoenung, J. M.; Lavernia, E. J. Thermal Behavior and Microstructural Evolution during Laser Deposition with Laser-Engineered Net Shaping: Part I. Numerical Calculations. Metall and Mat Trans A 2008, 39 (9), p. 2228–2236.